INTERNATIONAL ATOMIC ENERGY AGENCY
UNITED NATIONS EDUCATIONAL, SCIENTIFIC AND CULTURAL ORGANIZATION

INTERNATIONAL CENTRE FOR THEORETICAL PHYSICS
34100 TRIESTE (ITALY) - P.O.B. 586 - MIRAMARE - STRADA COSTIERA 11 - TELEPHONE: 2240-1
CABLE: CENTRATOM - TELEX 460392 - I

SMR.300/32

College on Medical Physics
(10 October - 4 November 1988)

Physical Principles and New Developments of Computed Tomography with Monoenergetic Radiation

R. CESAREO
Universita' di Roma "La Sapienza"
Centro Ingegneria Biomedica e Dipartimento di Energetica
Roma, Italy

1. Introduction

A series of transmission measurements of a collimated X or gamma ray beam through various and moving parts of a sample, obtained by translating and rotating the sample itself (Figure 1) give rise, after a mathematical process called reconstruction, to a map of distribution of physical densities in the section crossed by the incident beam. This map is called computer assisted tomograph (CAT) and the relative equipment, CAT-scanner.

A CAT-scanner is composed of different parts:

- an X or gamma-ray source and detector;
- a system for translating and rotating the sample;
- a computer for the reconstruction and visualization of the image.

The image is constituted by a map showing, in terms of darkness levels, the distribution of the attenuation coefficients in all pixels of the crossed section. The characteristics of the image is then depending on the difference between the attenuation coefficients of the components of the sample versus energy.

In Section 2 there are descriptions of the main interaction processes of X-rays with matter, in Section 3 the physicsl principles of CAT and in Section 4 the experimental apparatus realized in Rome. In Sections 5 and 6 two recent developments are described concerning differential tomography and Fluorescence X-Ray Tomography.

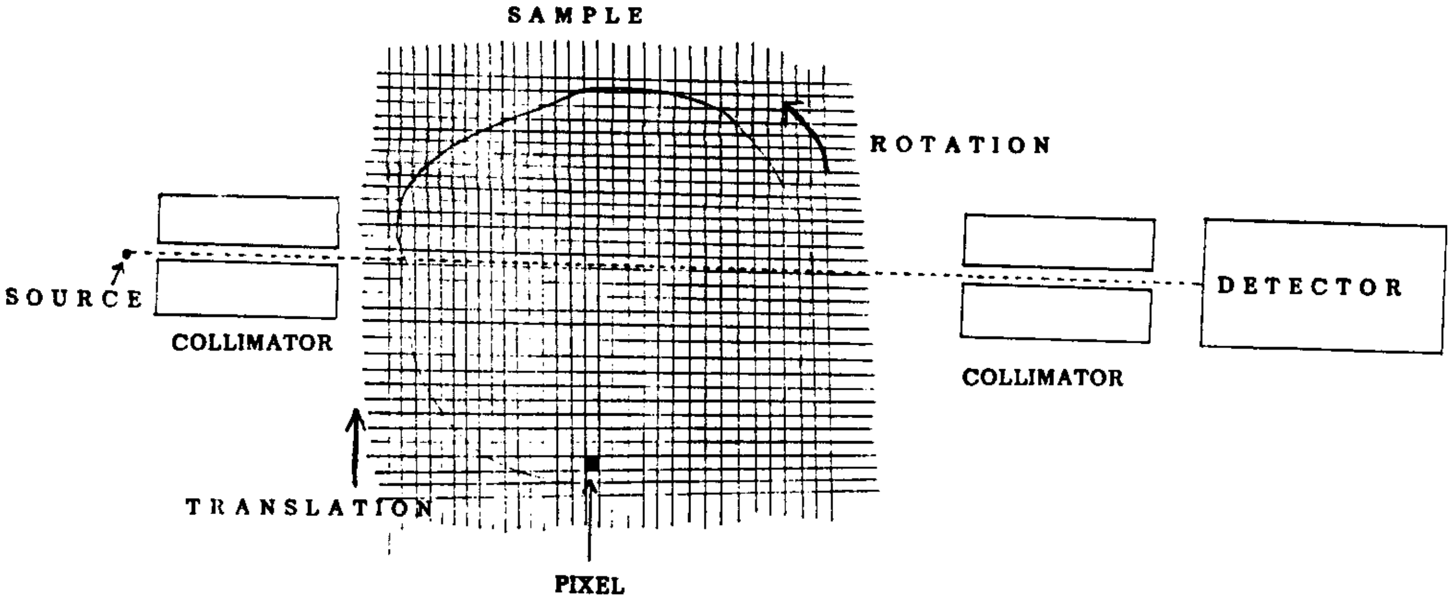

Figure 1 - Principles of the computer assisted tomography (CAT).

2. Interaction of radiation with matter.

Although a large number of possible interaction mechanisms are known, when monoenergetic X or γ-rays from about 10 to 500 keV are attenuated in matter, only three major effects are important: elastic or Rayleigh scattering, Compton effect and photoelectric effect.

These processes are dominant in different ranges of incident photon energy E_o as a function of mean atomic number of the sample. For example, the total attenuation of 10 to 500 keV energy radiation in water or equivalent material is shown in Figure 1'. This figure gives the contribution in percentage of these three interaction effects as a function of energy. Compton effect is dominant from about 50 keV, while photoelectric effect is more prominent at energies below 25 keV. Compared with the other two effects, elastic scattering contributes very little to the total attenuation, reaching a maximum of 10% of the total. However, E.S. may dominate in the forward direction (see Figure 5).

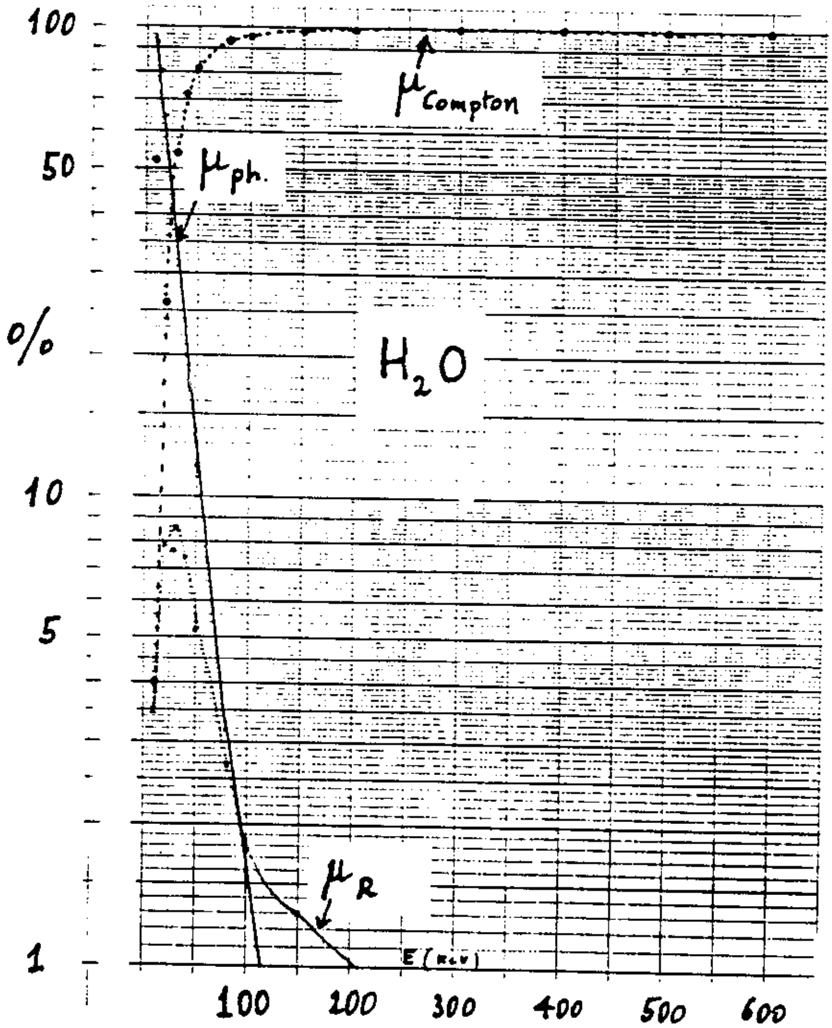

Figure 1' - Interaction of low energy radiation (10-600 keV) with matter. Relative contribution of photoelectric, Compton and elastic scattering effects are shown.

2.1 COMPTON EFFECT

The Compton scattering takes place between the incident X or γ-rays with energy E_o and an electron in the scattering material. This effect gives rise to a secondary electron and a photon with energy E_c, scattered through an angle ϑ with respect to its original direction. A scheme of this interaction is given in Figure 2.

The energy E_o of the incident photon is shared between the recoil electron and the scattered photon E_c. The energy of the scattered photon as a function of scattering angle ϑ is given by:

$$E_c = \frac{E_o}{1+\alpha(1-\cos\vartheta)} \tag{1}$$

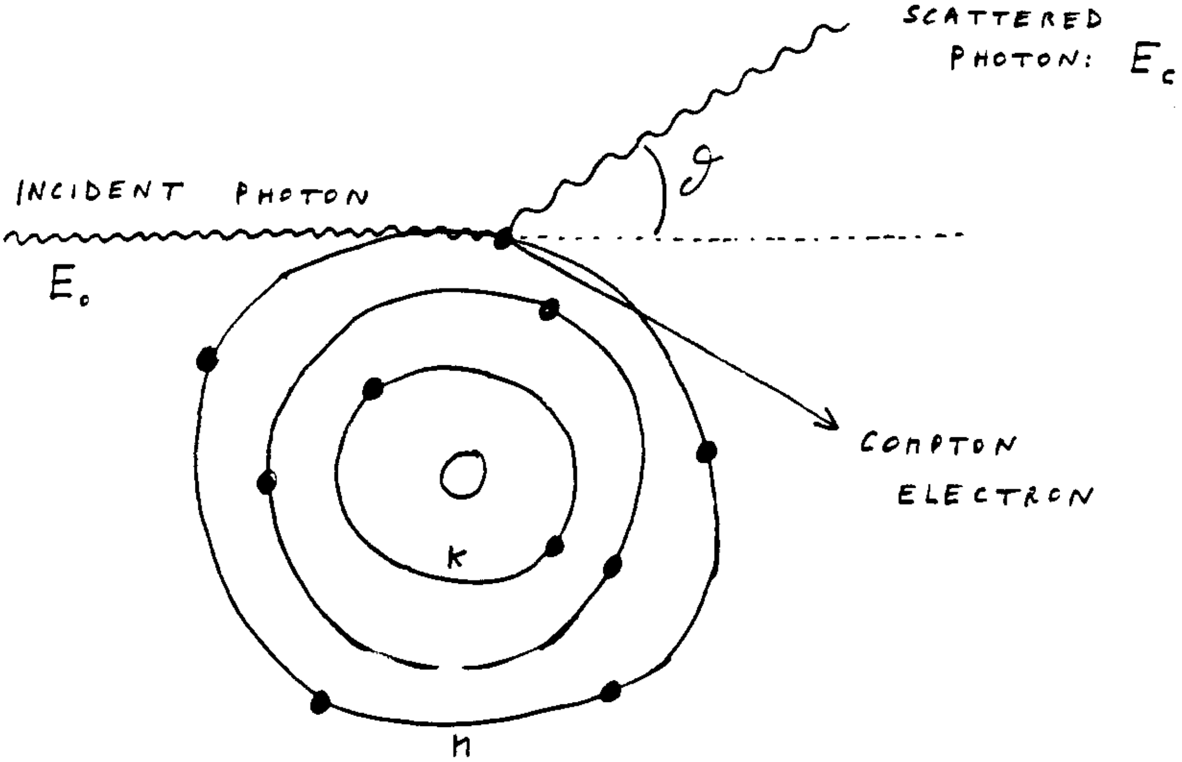

Figure 2 - Compton scattering of an X or gamma photon in which part of the incident photon energy is transferred to an electron of an absorbing atom. The remainder of the incident energy is retained by the scattered photon.

where $\alpha = E_0/m_0 c^2$ is the reduced energy of the incident photons and $m_0c^2 = 511$ keV is the rest mass energy of the electron. The scattering angle can take on values anywhere between 0 and 180 degrees. Figure 3 shows the energy dependence of Compton scattered radiation E_c as a function of the scattering angle for two different incident photon energies. In case the Compton electron is absorbed in the material, there is no much interest from the analytical point of view, while the scattered photon can be used to obtain information about the nature of the absorbing material. The differential cross section for Compton scattering is well-described by the product of the Klein-Nishina free electron distribution and the incoherent scatter function S, which accounts for electron binding effects. The differential cross-section for Compton scattering by unpolarized photons and per electron of scattering material is then given by:

$$\frac{d\sigma}{d\Omega} = \frac{r_0^2}{2}\left\{\frac{1}{\left[1+\alpha(1-\cos\theta)\right]^2}\left[1+\cos^2\theta+\frac{\alpha^2(1-\cos\theta)^2}{1+\alpha(1-\cos\theta)}\right]\right\}S(X,Z) \qquad (2)$$

where $\alpha = E_0/m_0c^2$; $r_0 = \frac{e^2}{m_0c^2} = 2.8\text{x}10^{-13}$ cm and $S(X,Z)$ is the incoherent scattering function in which X represents the momentum transfer parameter:

$$X = \frac{\sin\theta/2}{\lambda} \qquad\qquad \lambda = \frac{12398}{E_0(\text{eV})}$$

The value of $S(X,Z)$ varies between 0 and Z. When $X \longrightarrow 0, S \longrightarrow 0$, when $X \longrightarrow \infty$, $S \longrightarrow Z$.

The incoherent scattering functions are tabulated in ref. (1) and are reported in Figures 4. Figures 5 show the differential scattering (Eq. 2) as a function of the scattering angle for a biological matrix (water).

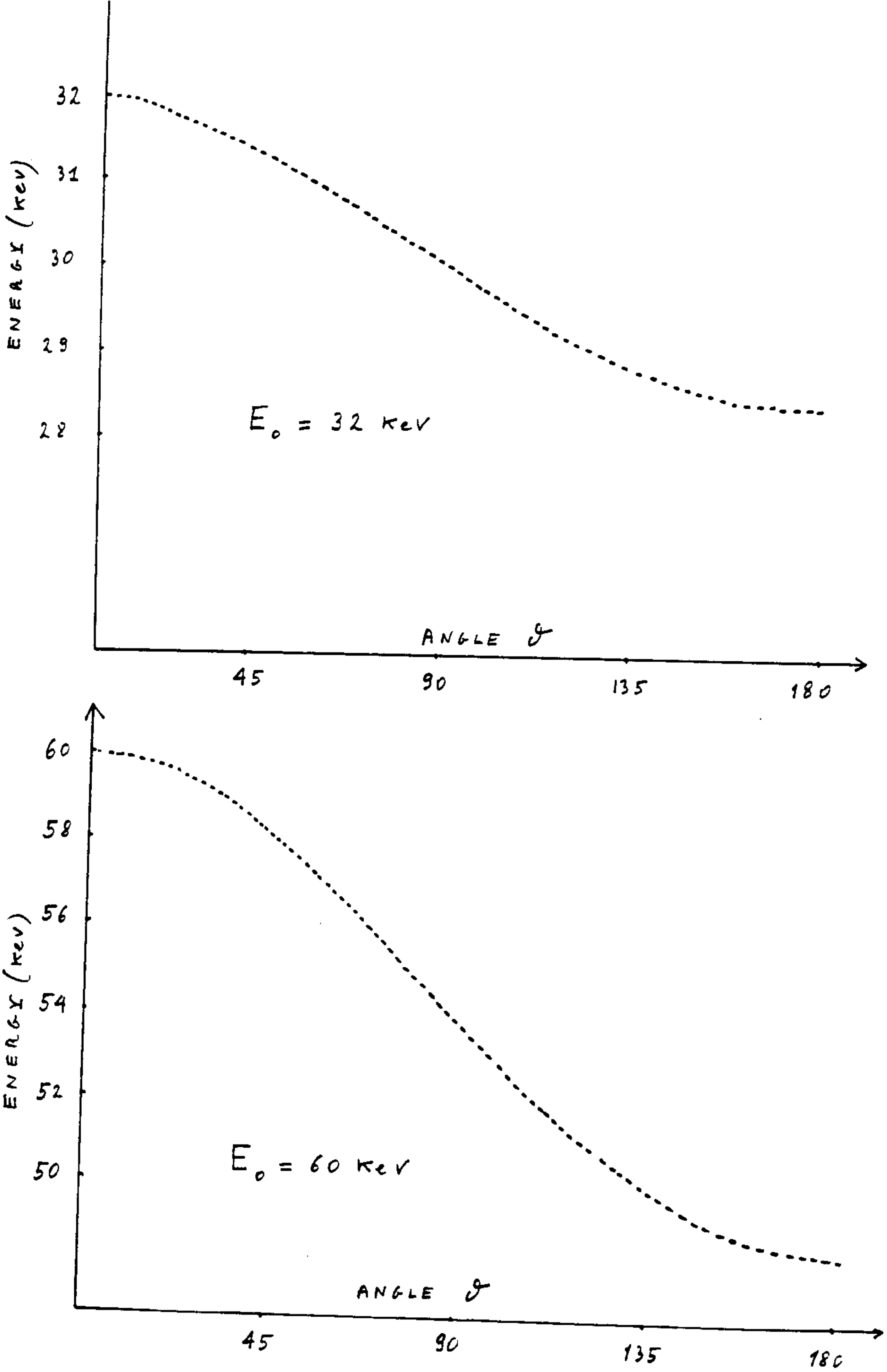

Figure 3 - Energy dependence of Compton scattering as a function of the scattering angle for incident radiation of 32 keV and 60 keV.

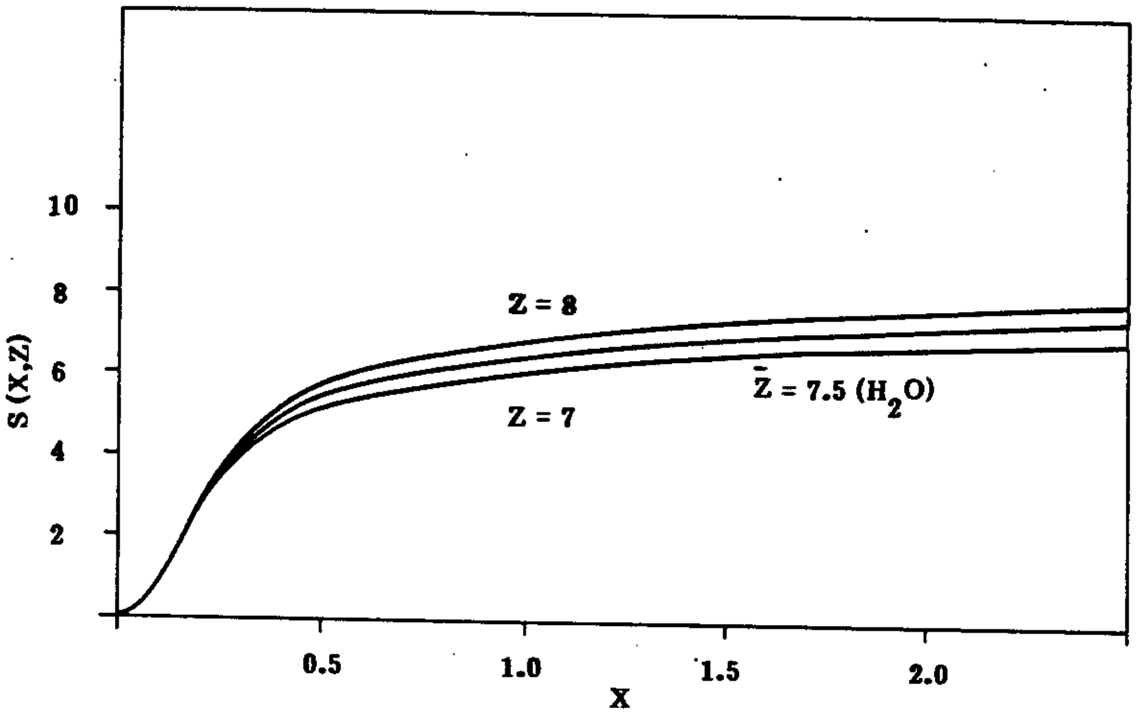

Figure 4 - Incoherent scatter function S(X,Z) versus momentum transfer parameter X for Z=7 (nitrogen), Z=8 (oxygen) and $\bar{Z}$ = 7.5 (water).

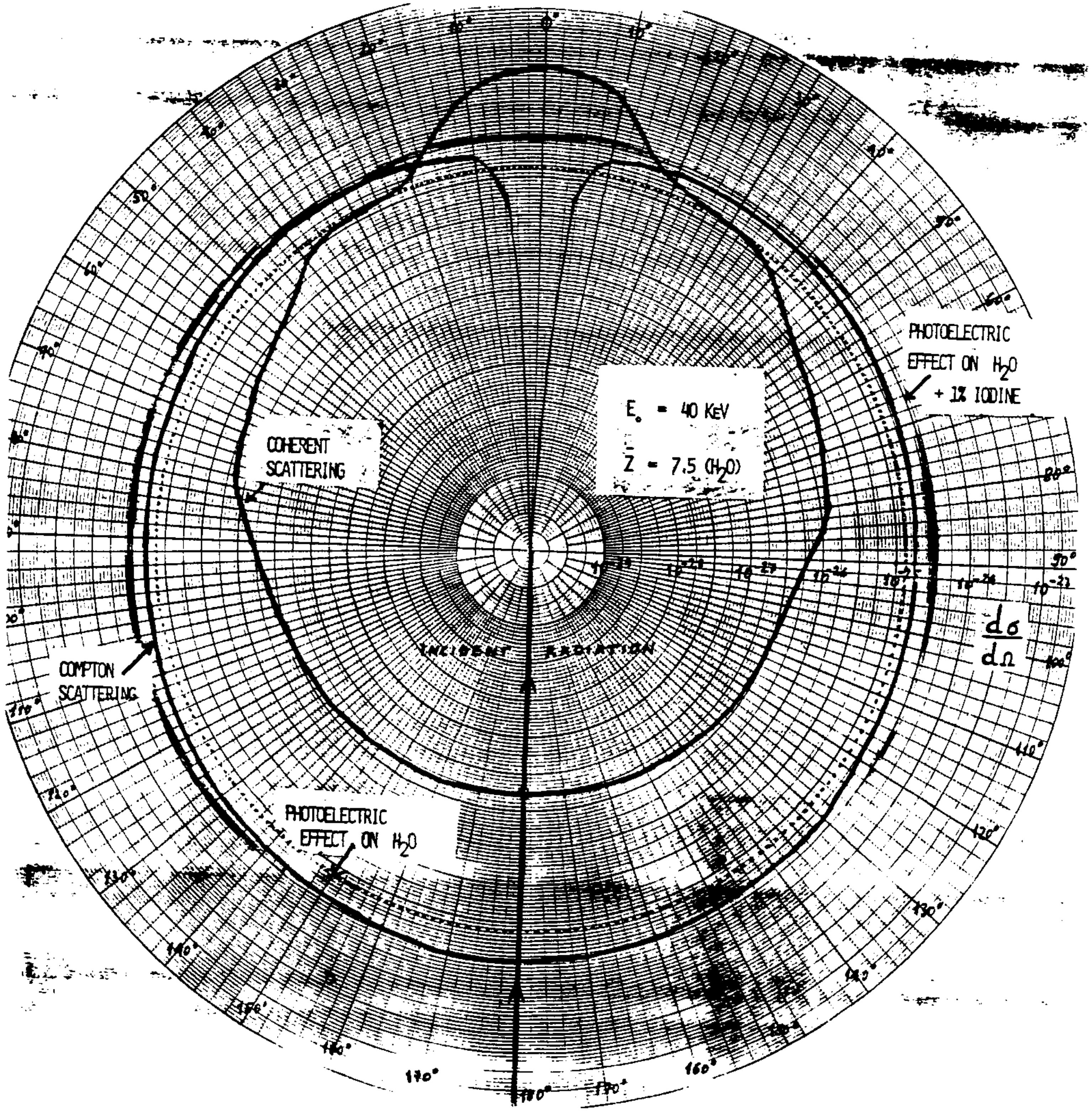

Figure 5 - Differential cross section of Compton, photoelectric and Rayleigh effects versus angle for incident energies of 40 keV in water.

2.2 RAYLEIGH SCATTERING

Rayleigh or coherent scattering is described in classical terms as the diffraction of an electromagnetic wave by the electric field associated with the electron charge distribution (Figure 6).
Let us introduce the classical Thompson differential cross-section for scattering from a free electron

$$\frac{d\sigma_{Th}}{d\Omega} = \frac{r_o^2}{2}\,(1+\cos^2\vartheta) \qquad (3)$$

When the electromagnetic wave excites more than one electron, the coherent scattering from different electrons shows interference effects. The scattering effect from a free atom with Z electrons is, therefore, not simply Z times the free electron amplitude.The most widely used approximation for calculating the coherent scattering cross-section is the atomic form factor approximation which is described in detail elsewhere.

The angular distribution per unit solid angle of coherent scatter for an atom is given by the product of the classical Thompson free electron cross-section and the square of the atomic from factor F, describing how free electron scatter is modified through inter-electron interference:

$$\frac{d\sigma_R}{d\Omega} = \frac{r_e^2}{2}\,(1+\cos^2\vartheta)\,\left[F(X,Z)\right]^2 \qquad (4)$$

The function F(X,Z) varies from F(0,Z)=Z to F(∞,Z)=0. Therefore , the coherent scattering is extremely forward peaked, and becomes more so as the energy is increased.

The atomic form factor can be found tabulated as a function of energy of the incident radiation E_0 scattering angle ϑ , and atomic number Z of the scattering material. Factors F(X,Z) are tabulated in ref. (1) and reported in Figure 7.

The form-factor approximation, based on semiclassical theory can led to appreciable errors for large Z-atoms or photon energies comparable to the electron rest mass energy. For light atoms and X-ray energies the form factor approximation is satisfactory.

Further, Equation (4) holds if multiple scattering effects are not important, that is, attenuation in the target material is negligible. Figures 5 show the differential cross section for coherent scattering, calculated from Equation (4). It can be observed that most of the coherent scattered photons are in the forward directions, and this effect increases with the energy of incident radiation and with the decreasing of the atomic number Z.

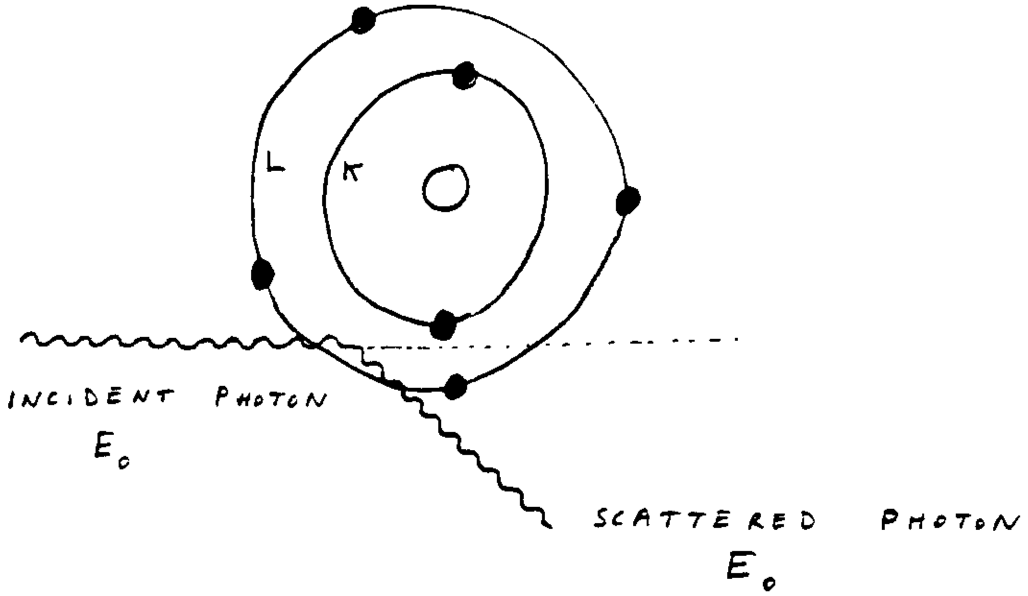

Figure 6 - Elastic or Rayleigh scattering in which an incident photon is scattered with negligible energy loss after interaction with the cloud of electrons in an atom.

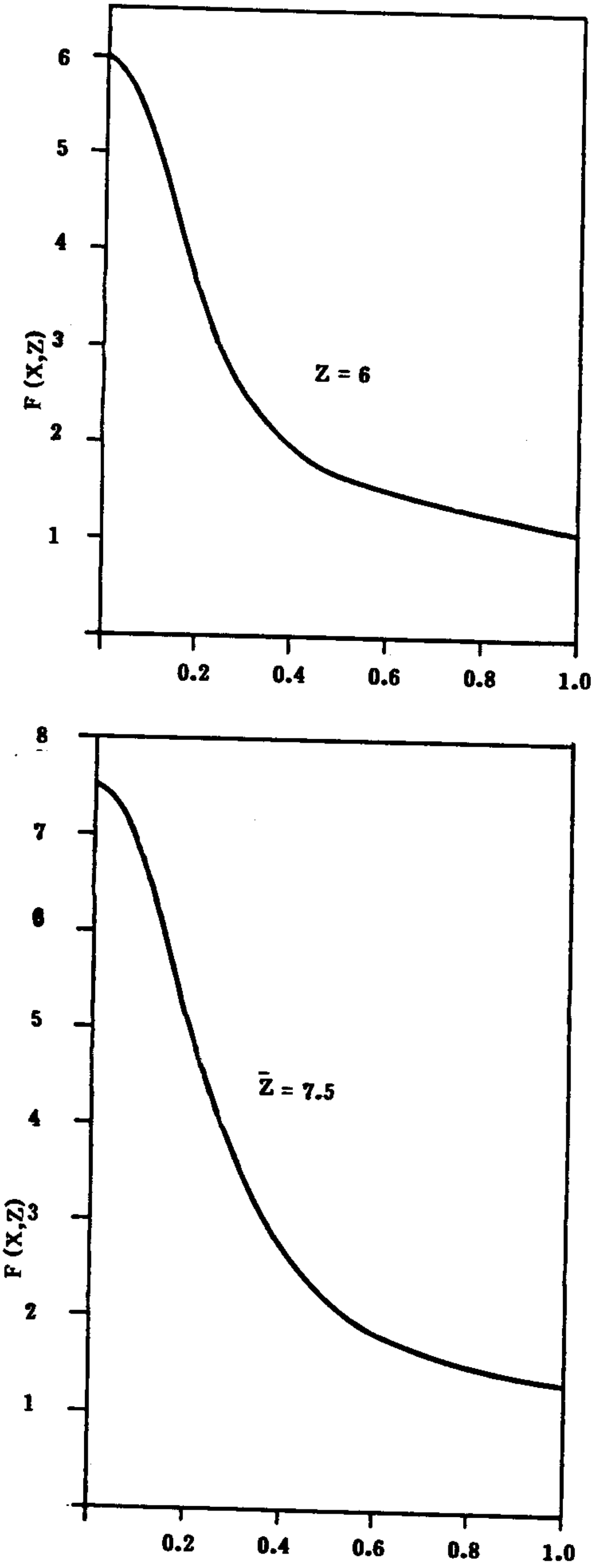

Figures 7 - Atomic form factor F(X,Z) versus momentum transfer parameter X for Z=6 (carbon) and $\bar{Z}$= 7.5 (water).

2.3 Photoelectric effect.

The photoelectric effect is the predominant X or γ-ray interaction, in medium and high Z absorbers, when the energy of incident radiation is below 100 keV.

In this process, the incident photon is absorbed by the scattering material and an electron from one of the inner electron shells (K or L) is ejected from the atom with the energy $T = E_o - BE$, where T is the kinetic energy and BE is the binding energy of the photoelectron. The vacancy in the atomic shell is filled by an electron from a less tighly bound electronic shell of the atom. Simultaneously, characteristic X-rays are emitted by the atom or, by an alternative process, Auger electrons.

Schematically, the photoelectric process is shown in Figure 8

The ratio between the probabilities of emission of characteristic X-rays to Auger electrons is called fluorescence yield. This is nearly zero for low-Z elements and nearly 1 for high-Z elements. The detection of these secondary X-rays, which are characteristic for each element, is the basis for the analytical technique known as X-Ray Fluorescence (XRF) analysis.

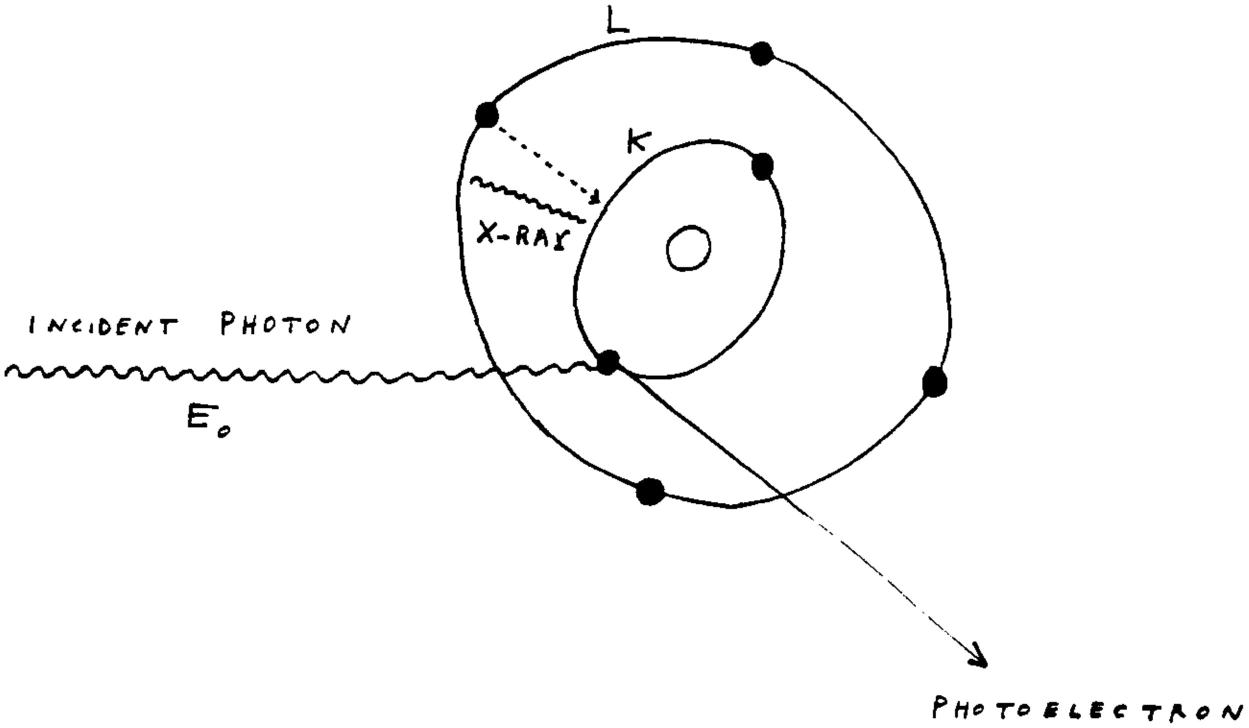

Figure 8 - Photoelectric effect, in which the energy of an incident photon is transferred completely to an electron. The electron is ejected from the atom with a kinetic energy $T = E_o - BE$ where BE is the binding energy of the electron. The vacancy in the atomic shell (K-shell in the Figure) is filled by an electron from an outer shell (L-shell in the Figure) and X-rays are emitted having energy $BE_K - BE_L$.

from the scattering angle, is shown in Figure 5.

The P.E. mass-attenuation coefficient for photons with incident energies below 100 keV, show characteristic discontinuous jumps known as absorption edges corresponding to the minimum energy for the ejection of electrons from its shells. For example, considering the photoelectric cross-section of iodine versus energy (see Figure 9), L-discontinuities are at 4.56 keV (L_{111}), 4.86 keV (L_{11}) and 5.19 keV (L_1), while the K-discontinuity is at 33.164 keV.

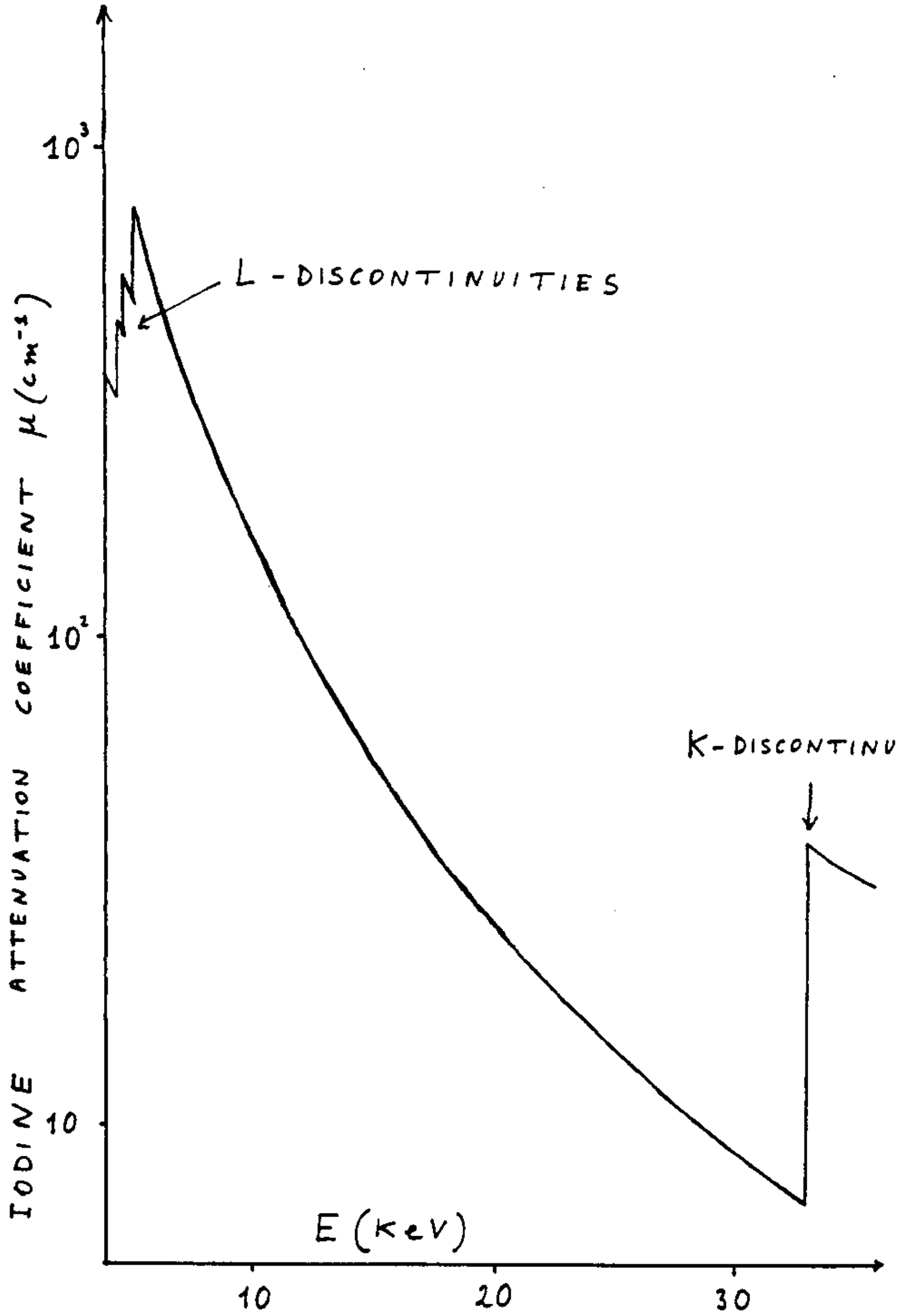

Figure 9 - Attenuation coefficient of Iodine (in cm^{-1}) versus energy showing the L-discontinuities and the K discontinuity of the photoelectric component.

When a narrow beam of monoenergetic photons with energy E_o and photon flux density (number of photons per unit area and time) N_o crosses a homogeneous absorber of thickness X, the emerging photon flux density N is given by:

$$N = N_o \exp\left[-\mu(\rho,Z,E_o)x\right] \qquad (5)$$

where μ(in cm^{-1}) is the linear attenuation coefficient for material of physical density $\rho(g/cm^3)$ and atomic number Z.
For energy values greater than about 10 keV, when molecular binding energies are small, it is reasonable approximation to assume that μ is directly proportional to the physical density and write:

$$N = N_o \exp\left[-\mu(Z,E_o)/\rho\right] \rho x \qquad (6)$$

where $\mu(Z,E)$ is the mass attenuation coefficient (in cm^2/g). If the absorber is a chemical compound or a mixture, its mass attenuation coefficient μ/ρ can be approximately evaluated from the coefficients for the constituent elements

$$\mu/\rho = \sum_i w_i(\mu_i/\rho_i) \qquad (7)$$

in which w_i is the proportion by weight of the i-th constituent.
The mass attenuation coefficient is also proportional to the total photon interaction cross-section per atom σ^a_{total} (in cm^2/atom) that is the sum of the cross sections for all the elementary scattering processes cited in Section 1.
The correlation between attenuation coefficient and atomic cross-section is the following:

$$\mu/\rho = \sigma^a_{tot.}\left(N_a/A\right) \qquad (8)$$

where N_a is the Avogadro's number and A the atomic mass of the absorber. Since there are Z electrons per atom

$$\mu/\rho = \sigma^{e}_{tot.}\left(\frac{N_a Z}{A}\right) = \sigma^{e}_{tot.} \ \delta_e \qquad (9)$$

where $\sigma^{e}_{tot.}$ (cm^2/electron) is the total cross section per electron and the term $\frac{N_a Z}{A}$ represents the electron density (number of electrons per gram).

For all elements except hydrogen, δ_e approximately equals $N_a/2=3x10^{23}$ (Table 1). This indicates that atomic composition dependence of μ/ρ is principally related to that of $\sigma^{e}_{tot.}$. There is, in Eq. (9) an approximate dependence of μ on Z in ρ and an expressed dependence on Z in δ_e.

Considering now the three effects contributing to the attenuation coefficient, from Eq. (9):

$$\mu = \rho\delta_e(\sigma^{e}_{R} + \sigma^{e}_{c} + \sigma^{e}_{ph}) \qquad (10)$$

It should be observed that, at a fixed energy, σ^{e}_{c} is approximately constant versus atomic number Z (Table 2) and the contribution of elastic scattering is lower than 10% of the total attenuation. Therefore, from Eq. (10):

$$\mu \simeq \rho\delta_e \ (K + K' Z^{\beta}) \qquad (11)$$

when K and K' are constant and $\beta \simeq 3 \div 4$.

In Eq. (11) are now explicitely separated the contributions of physical density and atomic number. In the energy region where the Compton effect is prevailing:

$$\mu \propto \rho \qquad (12)$$

TABLE 1 - Electron density δe of various elements, compounds and mixtures.

Element	Atomic Number Z or formula	Electron density (el/cm^3)
Hydrogen	1	6 x 10^{23}
Carbon	6	3 x 10^{23}
Nitrogen	7	3.01 "
Sulfur	16	2.89 "
Potassium	19	2.93 "
Chromium	24	2.78 "
Iron	26	2.8 "
Zinc	30	2.76 "
Arsenic	33	2.65 "
Silver	47	2.63 "
Iodine	53	2.515 "
Lead	82	2.38 "
Compounds or mixtures		
Muscle	-	3.47 "
Blood	-	3.48 "
Fat	-	3.15 "
Polyethilene	$(CH_2)n$	3.17 "
Water	H_2O	3.35 "
Nylon		3.8 "
Lucite	$(C_5H_8O_2)n$	3.87 "
Bakelite	$(C_{45}H_{38}O_7)$	4.27 "
Teflon		6.33 "

TABLE 2 - Compton cross section per electron σ_c^e at 100 keV. For E $\ll$ 100 keV, $\sigma_c^e \simeq$ 0.5 barn.

Element	Compton cross section σ_c^e (barn)
Hydrogen	0.493
Carbon	0.493
Nitrogen	0.493
Sulfur	0.492
Potassium	0.493
Iron	0.492
Zinc	0.492
Tin	0.492
Iodine	0.492
Lead	0.493

and the Compton linear attenuation coefficient is linearly proportional to the mass bulk density of the absorber.

In the low energy region, where the photoelectric effect is prevailing:

$$\mu \propto Z^{(3\div4)} \qquad (13)$$

and the attenuation coefficient critically depends on the atomic number of the absorber. For biological samples, $\bar{Z} \sim 7\div8$, and for low energy values ($E_0=10\div30$ keV), $\mu \propto Z^{3.5}$; for bone ($Z \sim 13$) $\mu \propto Z^{3.2}$. Since a tomography is based on many narrow beam X-ray attenuation measurements, and gives rise to a map of attenuation coefficient, the qualitative and quantitative characteristics of the image should reflect the dependence of total attenuation coefficient on density and atomic number of the absorber. Therefore, in the energy region in which the Compton effect is prevailing ($E_0 \gtrsim 50$ keV for biological materials) the linear attenuation coefficient (and therefore the tomography as map of attenuation coefficient) is proportional to the physical density of the absorber, and in the energy range in which the photoelectric effect is prevailing ($E_0 \lesssim 20$ keV for biological materials) the linear attenuation coefficient is proportional to a power of the atomic number Z of the absorber ($\mu \overset{\sim}{\propto} Z^{3\div4}$).

One of the most important parameter of CAT is the "contrast resolution", which can be defined as the ability of the CT-scanner to reveal differences in the transmission of X-Rays through an object containing structures which differ only slightly. The contrast resolution depends on the difference in the attenuation coefficients of the different structures, which, on the other hand, depends on the energy of the incident monoenergetic X-Rays or on the distribution of X-Rays if bremsstrahlung radiation is employed.

For bettering the contrast resolution the difference in the attenuation coefficient should be improved, which mainly depends (see Eq. 11) on the Compton effect and on the photoelectric effect (Fig. 10). The first term varies slightly for elements or materials with contiguous atomic number Z as a function of energy, so that, for example for biological samples, the contrast resolution is almost the same at 60 or 100 or 500 keV, where the Compton effect is largely prevailing.
The photoelectric effect, on the other hand, is very critically dependent on the atomic number Z of the samples and on the incident energy E_o, so that, theoretically, the contrast resolution will improve by reducing E_o. But, when E_o is reduced, the attenuation coefficient increases, and therefore, the useful dimension of the object to be scanned will be reduced too, according to the practical rule

$$\mu X \simeq 1 \div 6 \qquad (14)$$

Further, the radiation absorbed in the object will also increase, so as the absorbed dose. That limits the usefulness of employing radiation of reduced energy, for "in vivo" tomographs. The suggestion of using radiation of energy in the photoelectric effect region is therefore very useful for "in vitro" tomographs of objects of dimensions in accord with Eq. (14).
In a more general treatment, the contrast resolution is connected with: geometrical resolution (capacity to distinguish small structures); source intensity and source energy; total run-time T (in s); beam collimation.
When the contrast resolution is expressed in terms of $\Delta\mu/\mu$ (relative accuracy of the measured attenuation coefficients) it can be shown that (ref. 2):

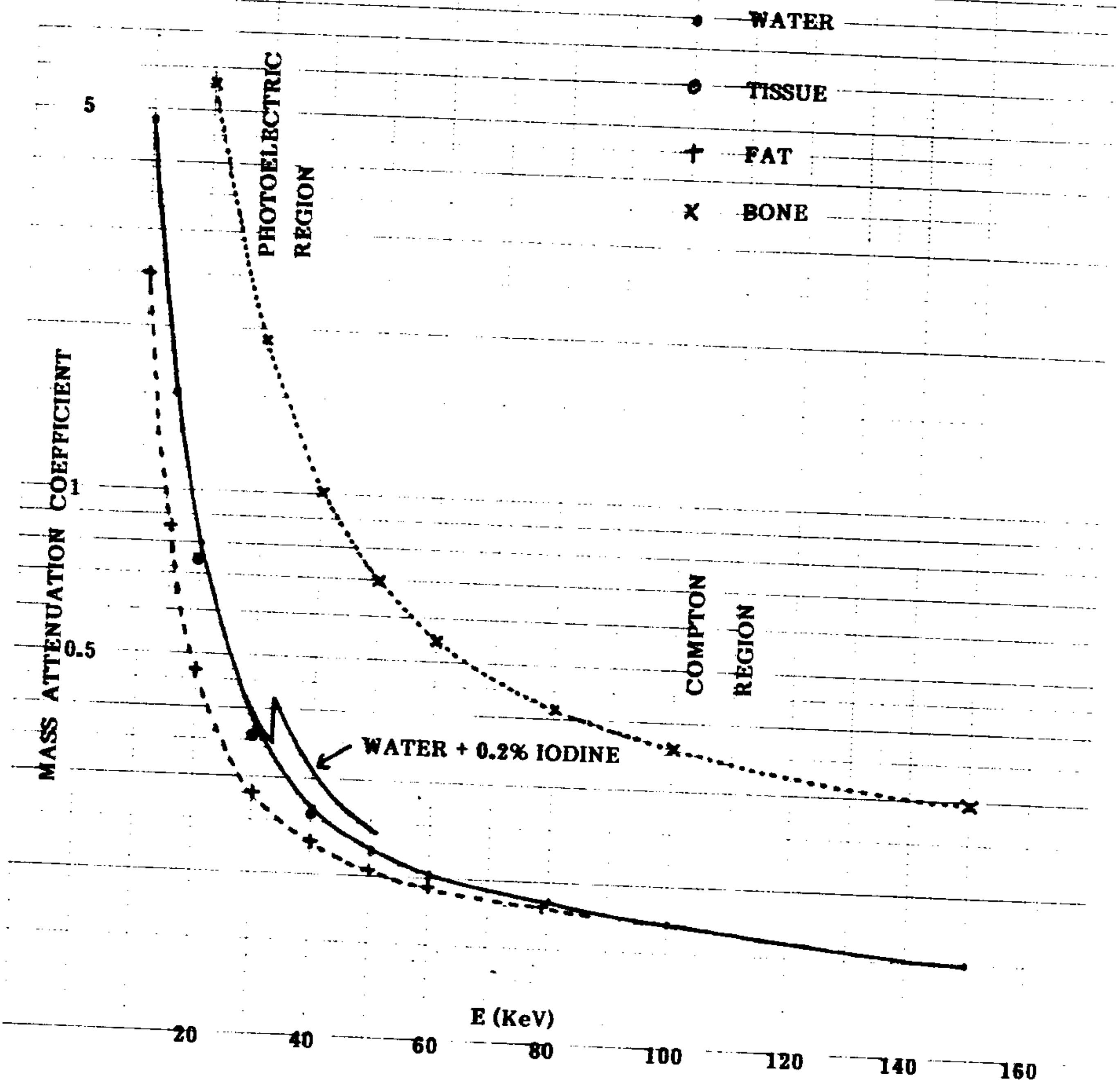

Figure 10 - Mass attenuation coefficient of water, tissue, fat, bone and water + 0.2% Iodine, versus energy. The region of prevailing photoelectric effect and Compton effect are shown.

$$\frac{\Delta\mu}{\mu} \simeq \frac{1.2\ N^{5/2}}{\sqrt{T}\ \sqrt{N_1}} \qquad (15)$$

when Eq. (14) is valid. In Eq. (15) NxN= number of pixels and N_1 = photons/s emitted by the source.
If for example N = 50, T = 3600 s, $\Delta\mu/\mu = 10^{-2}$, $N_1 = 10^9$ph/s.By defining $N_{tot.} = N_1.T$ as the total number of photons emitted by the source, Eq. (15) can be written as:

$$\frac{\Delta\mu}{\mu} = \frac{1.2\ N^{5/2}}{\sqrt{N_{tot.}}} \qquad (16)$$

For a given total photon flux $N_{tot.}$, an improvement in the contrast resolution can only be obtained by a reduction of the number of projection N, which is connected with the thickness of the beam.
The total number of photons (N_{tot}) emitted by the source versus the number of projections N, which gives rise to a fixed contrast resolution $\Delta\mu/\mu$ is shown in Figure 11.

4. Experimental set-up

The CAT-scanner developed at the Centro per l'Ingegneria Biomedica and employed for carrying out tomographs with monoenergetic radiation, differential tomographs and, see Par. 6 , fluorescence X-ray tomographs, is schematically shown in Figure 12 . It is characterized by:

- monoenergetic sources obtained both with radioisotopes and with X-ray tubes with secondary targets
- NaI (Tl) - X-ray detectors or a HP-Ge detector (for differential tomography)
- a translation-rotation system
- an electronic chain with a multiscaler
- a PC-Apple II E with reconstruction programmes working in Pascal.

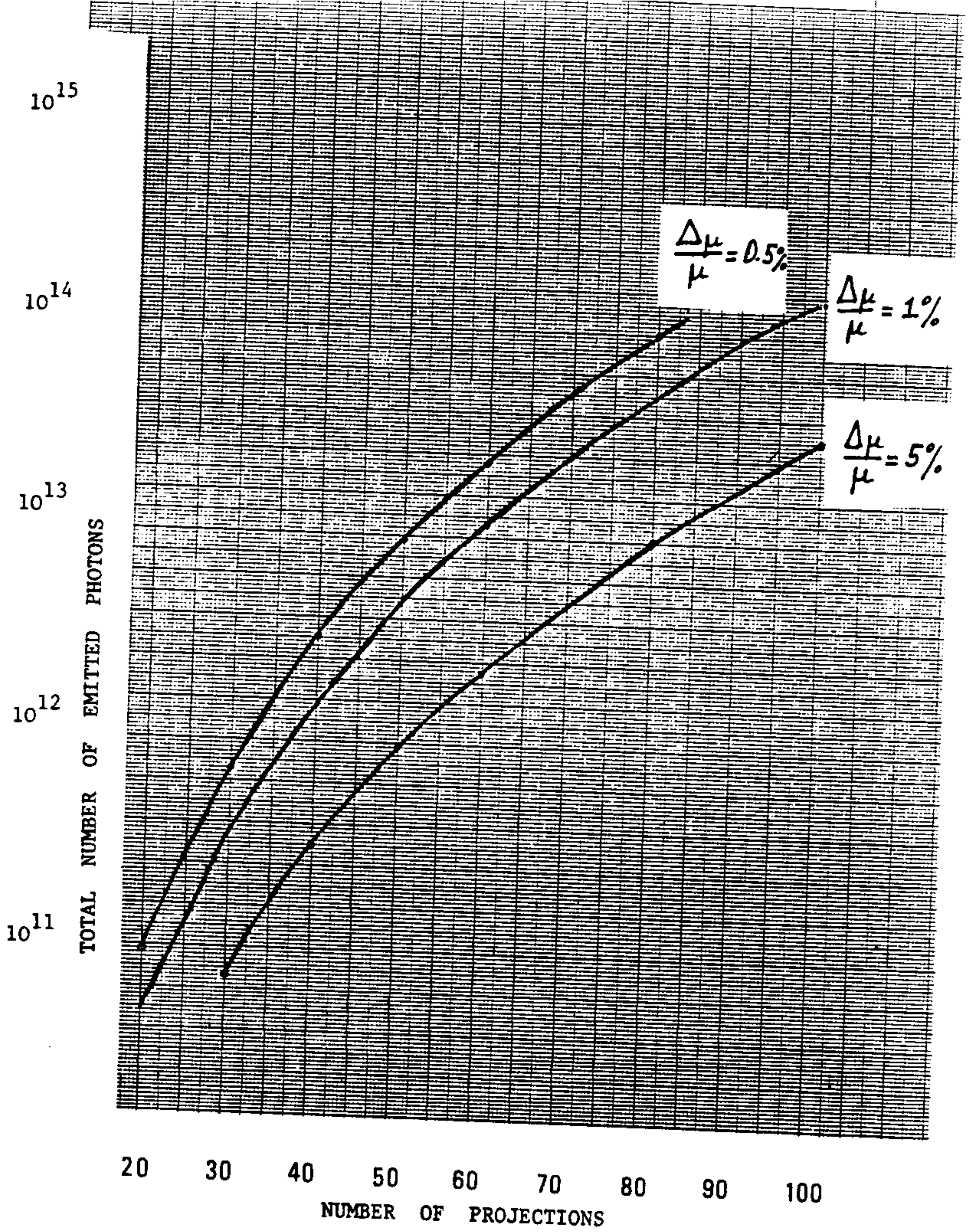

Figure 11 - Relative contrast resolution $\Delta\mu/\mu$ versus number of projections and total number of emitted photons.

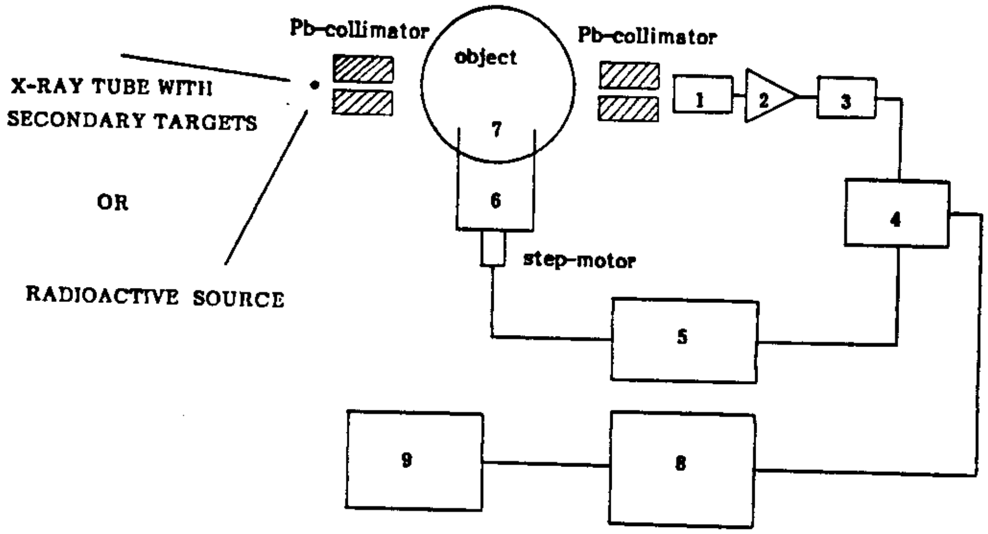

1. DETECTOR
2. AMPLIFIER
3. SINGLE CHANNEL ANALYZER
4. MULTISCALER
5. CONTROL UNIT FOR TRANSLATION AND ROTATION
6. STEP MOTOR
7. TABLE FOR TRANSLATION AND ROTATION
8. APPLE-II EUROPLUS
9. MONITOR.

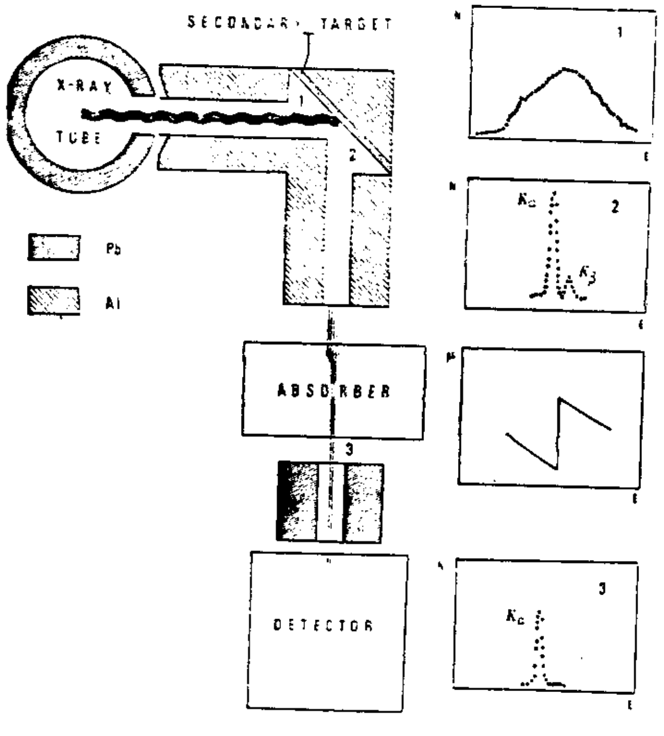

Figure 12 - Schematic set-up of the CAT-scanner developed in Rome at the "Centro per l'Ingegneria Biomedica" (top) and arrangement for converting the bremsstrahlung radiation from an X-ray tube in quasi monoenergetic radiation, by using secondary targets (bottom).

For testing the theoretical considerations of Section 3, and for carrying out differential tomographs (see Section 5), monoenergetic sources are required of high intensity. They can be obtained with:

1. radioactive sources
2. X-ray tubes with secondary targets
3. synchrotron radiation.

Only few radioisotopes emit one or more X or γ lines of proper half-life values:

Am-241, which emits 60 keV γ-rays with a half-life of 433y, Gd-153, which emits 97 keV and 103 keV γ-rays with a half-life of 211d, Cs-137, which emits 667 keV γ-rays with a half-life of 30y and Co-60 which emits 1170 and 1330 keV γ-rays with a half-life 5.3y. Radioisotopes are needed emitting more than 10^8 ph/s.

X-ray tubes with external, interchangeable secondary targets, are very useful for generating quasi monoenergetic radiation (K_α and K_β-rays emitted by the target) of various energy values and intensities. A scheme of the apparatus is shown in Figure 12.

Synchrotron radiation, when at disposal, offers a very good solution in the generation of high-intensity monoenergetic X-rays in the range 5-50 keV. Unfortunately, synchrotrons are uncommon, expensive and not so easy to manage.

Reconstruction of the tomographic image

As observed in Section 1, in a tomography hundreds or thousands of measurements are carried out of the transmission of X-rays through the sample. From these transmission measurements,a matrix of numbers is obtained related to linear attenuation coefficients.

If a fine beam of X-rays of intensity I_o is incident on a sample and the emerging intensity is I, then the quantity

$$g = \ln \left(\frac{I_o}{I}\right) = \int_L \mu \, d s$$

is obtained, when f is the variable absorption coefficient along the line L (figure 13).

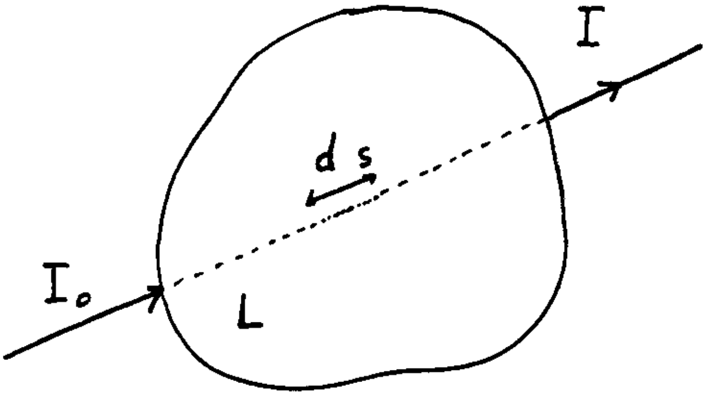

Figure 13

Hence, if g is known for all lines intefsecting the sample, and $\mu(x,y)$ is a function in two dimensions, the question is: can μ be determined if g is known? The answer is yes, it can, and a similar mathematical problem was first solved by Radon in 1917 (ref. 3) Only a conceptual explaination of the possible solutions is offered here. Three mathematical methods have been employed for reconstruction of medical images from X-ray transmission data. These methods are: 1) back-projection; 2) filtered back-projection and 3) iterative reconstruction.

1) back-projection

Suppose that the transmission of X-rays through an homogeneous cylindrical object is measured along two rays from two views at right angles to each other. X-ray transmission profiles are shown in Figures 14 .

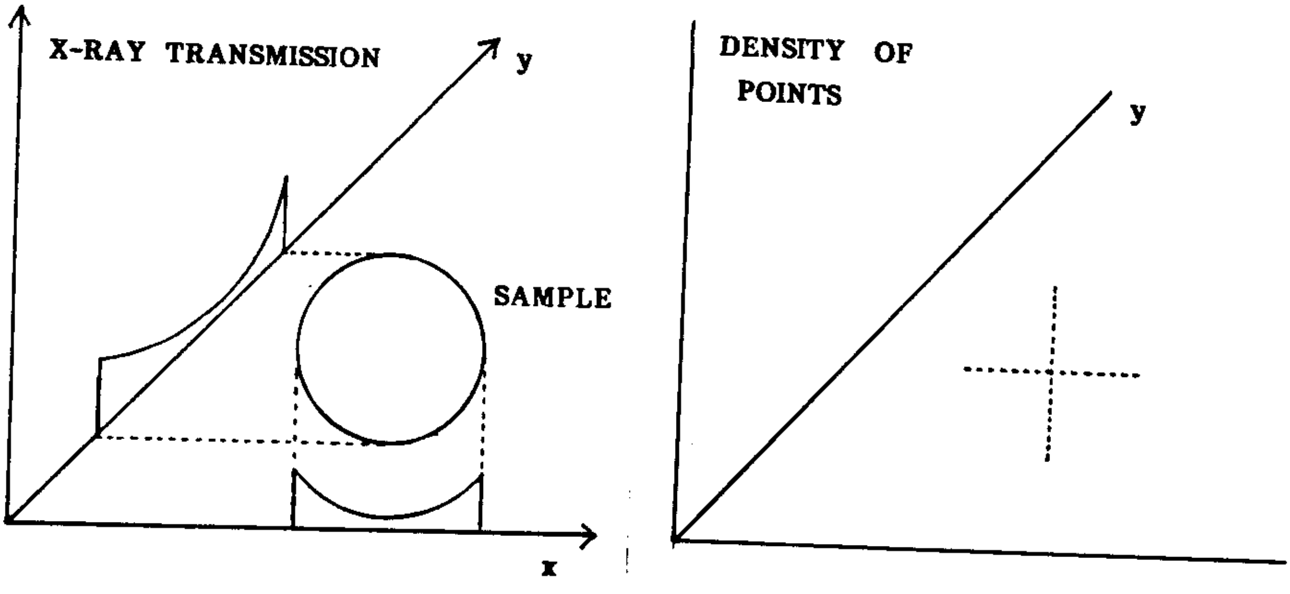

Figures 14 - Back-projection of a cylindrical homogeneous sample.

After the X-ray transmission profiles have been obtained, the process can be reversed, to form a crude image of the two rays (homogeneous density of points).

Let us suppose now that the object has a spherical volume of larger attenuation in the center; the X-ray transmission and the density profile are shown in Figures 15.

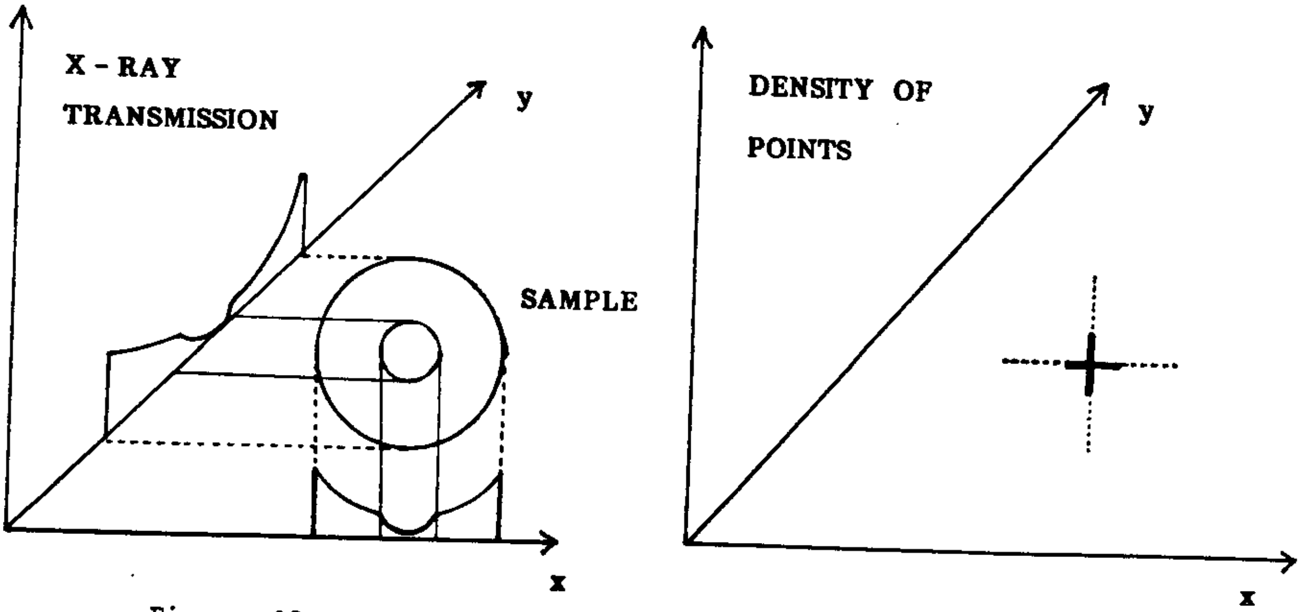

Figures 15 - Back-projection of a cylindrical inhomogeneous sample.

Simple back-projection can be explained in another way. Suppose that a series of X-ray transmission measurements are made at x and y orientations across a single plane through a cube (figure 16), resulting in the X-ray transmission data reported in the axes (14 measurements along the y axis and 10 measurements along the x axis).

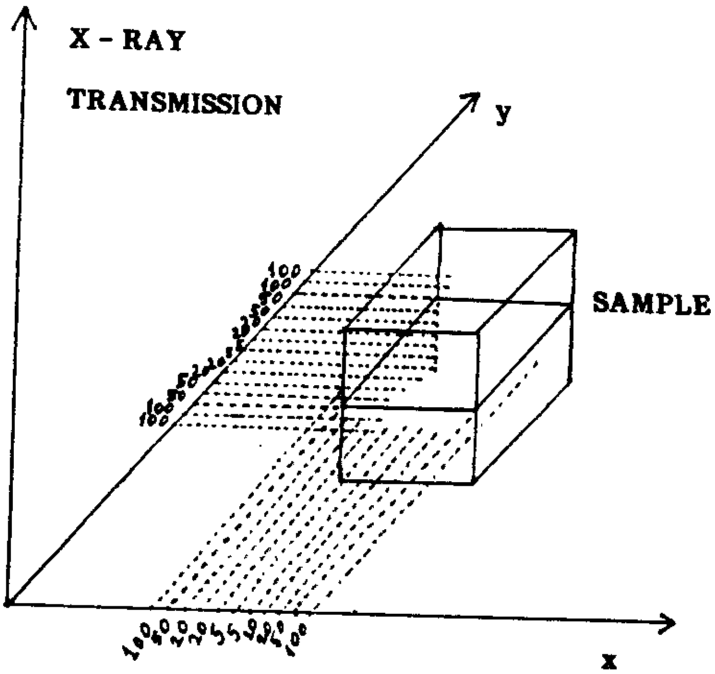

Figure 16 - Example for explaining back-projection.

Each transmission ray in the x-axis is divided into 10 parts and each ray in the y-axis into 14 parts (an area of 10 x 14 pixels is then delimited) and along the axis each ray reveals 5, 20, 50 and 100 percent transmission, corresponding to 95, 80, 50 and 0 percent attenuation, respectively.

Each part of the ray is assumed to contribute equally to the absorption. For example the ray transmitted along the x axis with a value of 5 is attenuated by 95%, and each of the 10 cells in the x axis contributed 9.5 percent. In Figure 16 these attenuation figures are added along the two axis, giving rise to the numbers shown in Figure 17 and to the image shown in Figure 18 .

The image would be not satisfactory, because the projected attenuations are averaged along the entire transmission ray and are not confined in the object of interest.

2) Filtered back-projection

To reduce spoke-pattern artifacts in back projected image, the X-ray transmission data can be modified (filtered) before they are analyzed to form an image. The filtering process adds negative components to the back projected data, so that the spokes are eliminated to a reasonable degree.

3) Iterative reconstruction

In this method,values initially are assumed for the matrix of attenuation coefficients used to form the image. As the transmission data are examined, corrections are made in the coefficients to achieve better agreement with the transmission data. This process is repeated many times in an iterative manner, with the corrections becoming smaller and smaller.

The iterative approach to image reconstruction is shown in Figure 19 .

0	3.6	5.7	5.7	6.8	6.8	5.7	5.7	3.6	0
0	3.6	5.7	5.7	6.8	6.8	5.7	5.7	3.6	0
5	8.6	10.7	10.7	11.8	11.8	10.7	10.7	8.6	5
5	8.6	10.7	10.7	11.8	11.8	10.7	10.7	8.6	5
8	11.6	13.7	13.7	14.8	14.8	13.7	13.7	11.6	8
8	11.6	13.7	13.7	14.8	14.8	13.7	13.7	11.6	8
5	13.1	15.2	15.2	16.3	16.3	15.2	15.2	13.1	5
5	13.1	15.2	15.2	16.3	16.3	15.2	15.2	13.1	5
8	11.6	13.7	13.7	14.8	14.8	13.7	13.7	11.6	8
8	11.6	13.7	13.7	14.8	14.8	13.7	13.7	11.6	8
5	8.6	10.7	10.7	11.8	11.8	10.7	10.7	8.6	5
5	8.6	10.7	10.7	11.8	11.8	10.7	10.7	8.6	5
0	3.6	5.7	5.7	6.8	6.8	5.7	5.7	3.6	0
0	3.6	5.7	5.7	6.8	6.8	5.7	5.7	3.6	0

Figure 17 - Application of back-projection on the sample of Figure 16. An homogeneous attenuation by each pixel along the ray is supposed.

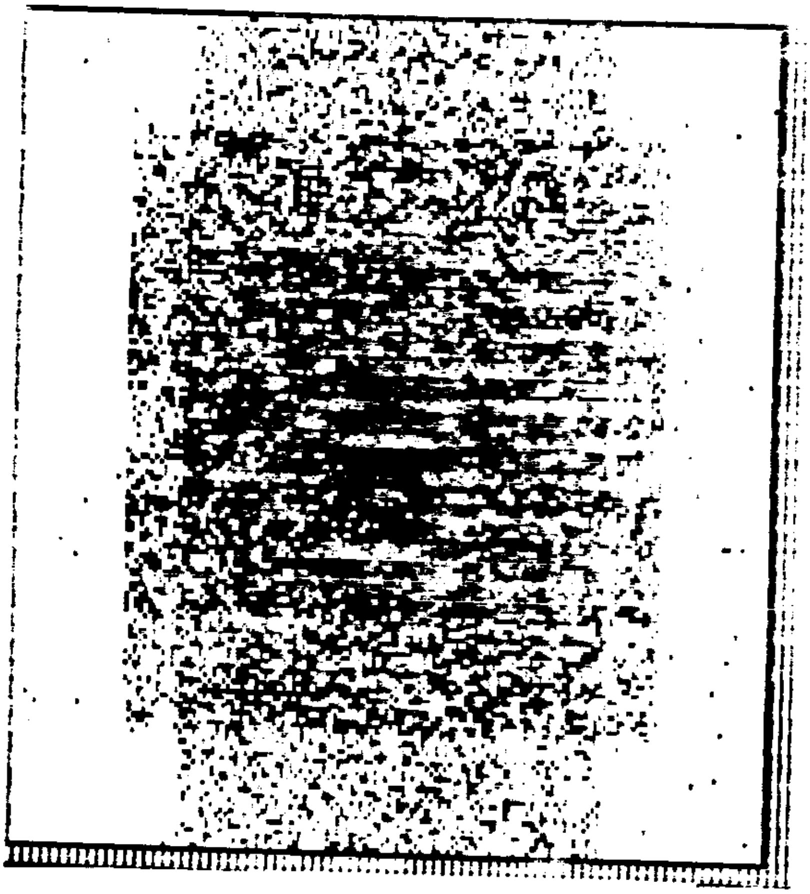

Figure 18 - Image of the sample shown in Figure 16 based on the numbers of Figure 17. Example of application of back-projection

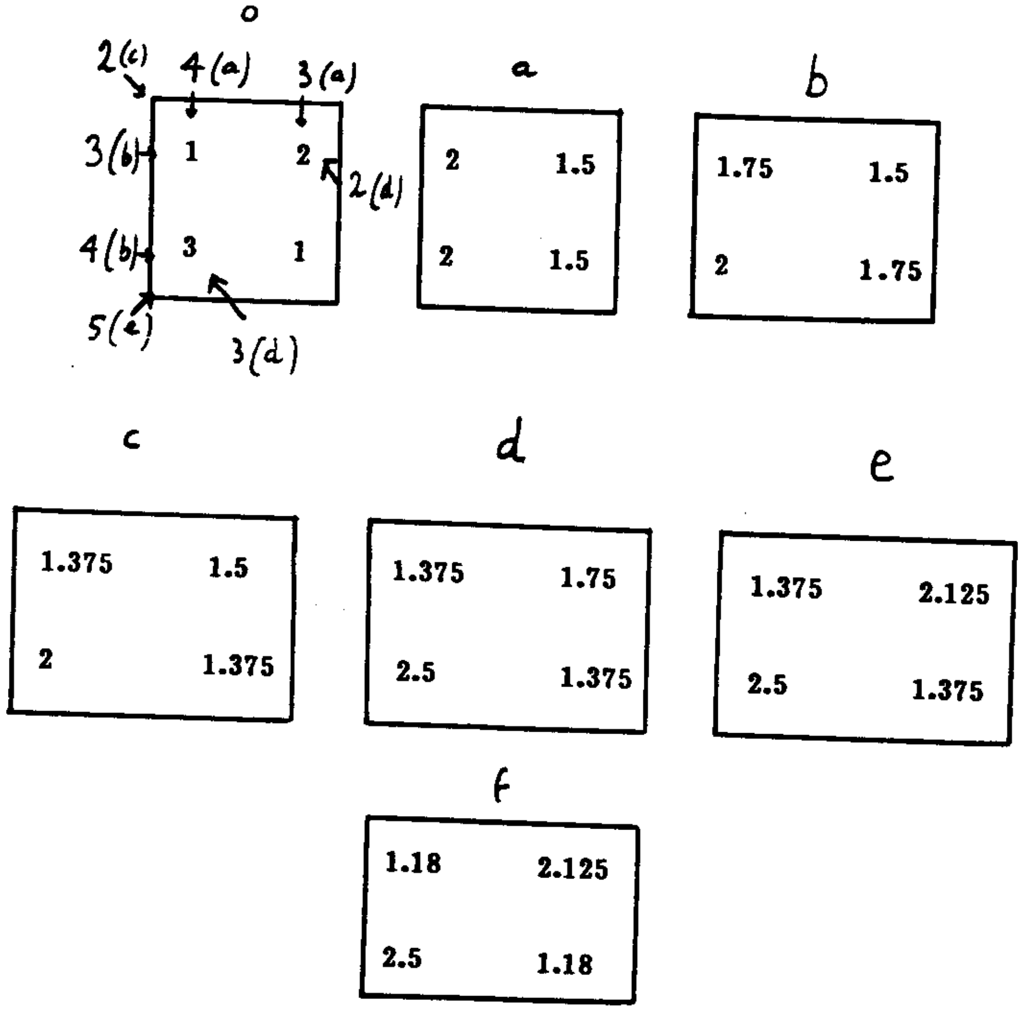

Figure 19 -Iterative approach to image reconstruction in a very simple case of a 2 x 2 elements matrix.Below,the images of steps 0,a,b,c,d and f.

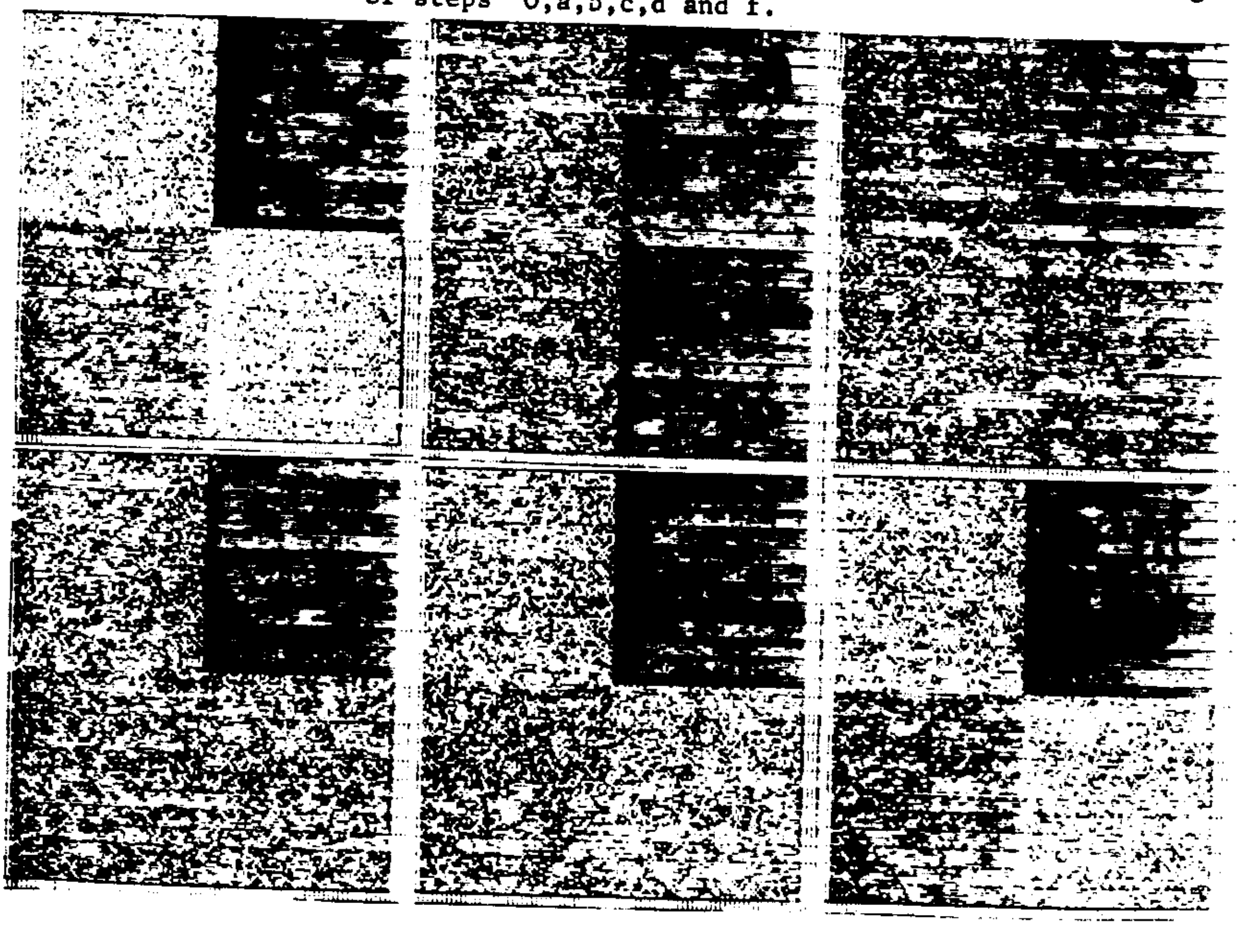

Attenuation coefficient of every element exhibits sharp discontinuities (K,L...) in correspondence with the minimum energy values for the ejection of the electrons from its shells (see Fig 20). For quantitative evaluation, values of attenuation coefficients of Fe, Ag, I and Pb near K and L-edges are shown in Table 3 . As can be observed, the difference in the attenuation coefficient above and below the edges varies between large values.

The discontinuities in the attenuation coefficient of an element can be employed for "amplifying" it presence in any sample, where attenuation measurements or tomographs are carried out with monoenergetic radiation having an energy value just above the energy of the edge (references 4 and 5).

Further, when two attenuation measurements are carried out with a pair of monoenergetic radiation which energy close brackets

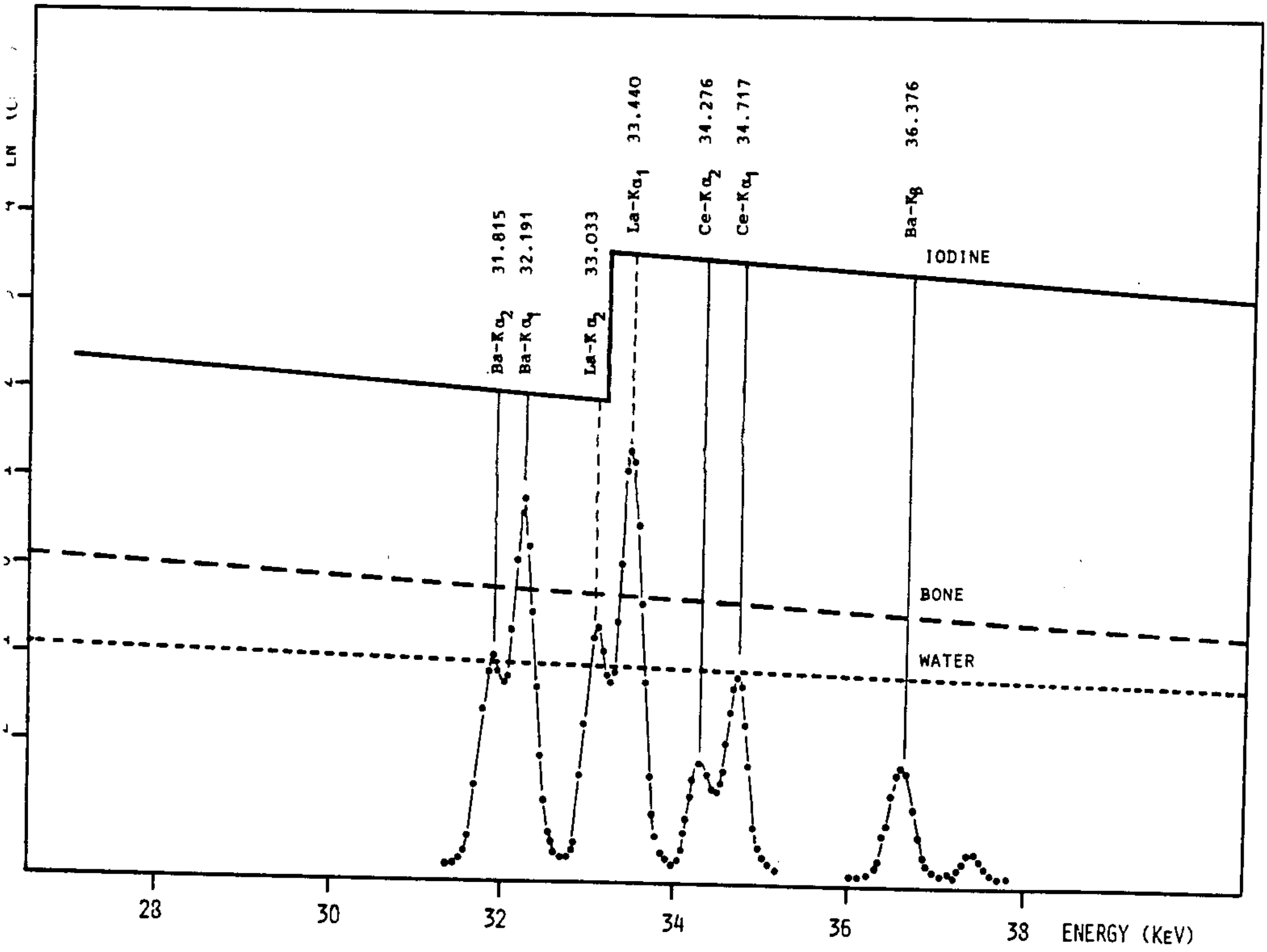

Figure 20 - Attenuation coefficient of Iodine, showing the K-discontinuity, and position of X-rays of Barium, Lanthanum and Cerium, useful for the differential tomography of Iodine.

TABLE 3 - Attenuation coefficient (cm^2/g) for Cu, Ag, I and Pb close to the discontinuities.

Element	Energy of the edge (keV)	μ_1	μ_2	$\Delta\mu$	F
Cu	8.98 (K)	28	285	257	215
Ag	25.52 (K)	9.7	52	42	1050
I	33.164(K)	7.5	32.5	25	5000
Pb	13.04(L_{III})	73	153	80	
	15.21(L_{II})	112	143	30	
	15.87(L_I)	136	141	5	
	88.0 (K)	1.8	6.6	4.8	400

the energy of the discontinuity, then the difference between the two measurements is only sensitive to the presence of the given element. This effect is well known since long time in radiology for the visualization of iodinated vessels (energy-dependent substraction angiography). In this case, no mono-energetic radiation is employed, but bremsstrahlung radiation at different HV-values.

5.1. Theoretical background

By considering a matrix of thickness x containing an element a with concentration c_a, the attenuation of incident monoenergetic radiation composed by a pair of X-rays of energy E_1 and E_2 respectively, which bracket the energy of the photoelectric edge of the element a, is given by:

$$N_1 = N_{01} \exp - \left\{ + \mu_{m1} + \mu_{a1} C_a \right\} x$$

$$N_2 = N_{02} \exp - \left\{ + \mu_{m2} + \mu_{a2} C_a \right\} x \qquad (17)$$

if $c_a \ll 1$. In Eqs. (17) N_{01}, N_{02}, N_1 and N_2 represent the intensity of incident and transmitted radiation of energies E_1 and E_2 respectively; μ_{m1} and μ_{m2}, μ_{a1} and μ_{a2} represent the attenuation coefficients of the matrix and of element a at energies E_1 and E_2 respectively. The ratio $R = \frac{N_2}{N_1}$ can be written as:

$$R = \frac{N_2}{N_1} = \frac{N_{02} \exp - \left\{ \mu_{m2} + \mu_{a2} c_a \right\} x}{N_{01} \exp - \left\{ \mu_{m1} + \mu_{a1} c_a \right\} x}$$

$$R = R_0 \exp - \left\{ \Delta\mu_m + \Delta\mu_a c_a \right\} x$$

where $R_o = \frac{N_{02}}{N_{01}}$, $\Delta\mu_m = \left(\mu_{m1} - \mu_{m2}\right)$, $\Delta\mu_a = \left(\mu_{a1} - \mu_{a2}\right)$

Close to the edge $\mu_{m2} \simeq \mu_{m1}$, $\mu_{a2} \gg \mu_{a1}$, and therefore $\Delta\mu_m \ll \Delta\mu_a$. If $\Delta\mu_a c_a \gg \Delta\mu_m$, then:

$$\ln \frac{R_o}{R} \simeq \Delta\mu_a c_a \; x \tag{19}$$

The ratio $\frac{R_o}{R}$ is only dependent on the concentration of element a. The effect of the matrix is proportional to the ratio:

$$F = \frac{\Delta\mu_m}{\Delta\mu_a c_a} \tag{20}$$

For example, when iodine is considered (E_{kab}= 33.169 keV) and E_1 = 32 keV (Ba-secondary target) and E_2=34.5 keV (Ce-secondary target), then:

$F = 0.027/30\ c_1$ and when E_1 = 33.033 keV (La-K $_2$ line) and E_2 = 33.44 keV (La-K $_1$ line), then $F = 0.007/30\ c_1$. Equation (19) is then valid when $c_I \gtrsim$ 0.9% in the first case and $c_I \gtrsim$ 0.2% in the second case.

Tomographs have been carried out at energies above and below the K-discontinuity of silver and iodine.

For silver, which has the K-discontinuity at 25.517 keV, secondary targets of tin (K_α =25.15 keV) and antimony (K_α = 26.2 keV) have been employed.

In Figure 21 are shown results of differential tomographs carried out on a plexiglas cylinder with two holes filled with Ag solutions at 4% and 2% (Fig.21A) and 1% (Fig.21B).

For iodine, which has the K-discontinuity at 33.164 keV, various pairs have been examined: Ba-K_α (32 keV) and Ba-K_β (36.4 keV); Ba-K_α (32 keV) and Ce-K_α (34.5 keV); La-$K_{\alpha 2}$ (33.033 keV) and La-$K_{\alpha 1}$ (33.44 keV). Tomographs using the last pair are shown in Figure 22.

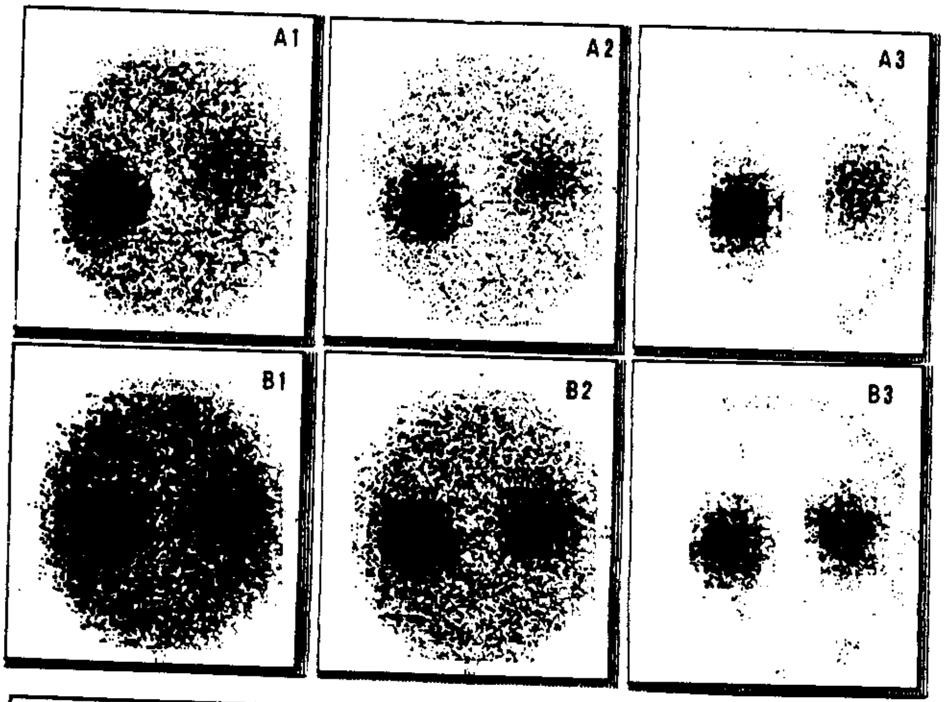

Figure 21-Differential tomographs on plexiglas cylinders containing Silver.

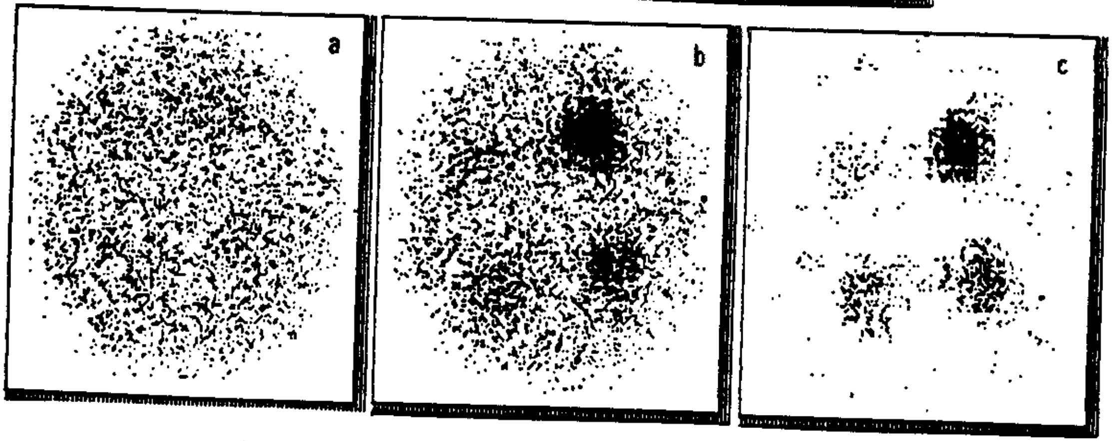

Figure 22 - Differential tomographs on plexiglas cylinders with 4 holes containing Iodine. Tomography a was carried out at 33.033 keV and tomography b at 33.44 KeV. The difference b-a exalts the iodine presence. I-concentration was 4, 2, 1 and 0.5% respectively.

6. Fluorescent X-ray tomography

This type of tomography is based on the detection of the fluorescent X-rays emitted by a sample containing elements with medium or high atomic number.(ref. 6).

The principle of the method is shown in Figure 23.

The output of the X-ray tube is strongly collimated by a collimator 6 cm long and 1 mm diameter which delimits in the object to be scanned a trunk of conical volume.

The detector, which analyzes the X-rays emitted by the irradiated volume, (a HpGe having 900 eV resolution at the Iodine X-rays) is placed at 90° with respect to the primary radiation, and is also collimated with a collimator very similar to the other one. The crossing of the solid angles of both collimators identifies a fixed volume in the object, which is approximately 2.5 x 2.6 x 2.5 mm^3. By moving the object in the x-y direction, X-ray intensity of elements present in the sample can be mapped, and finally an image can be obtained related to the distribution of the element or of the elements in the sample.

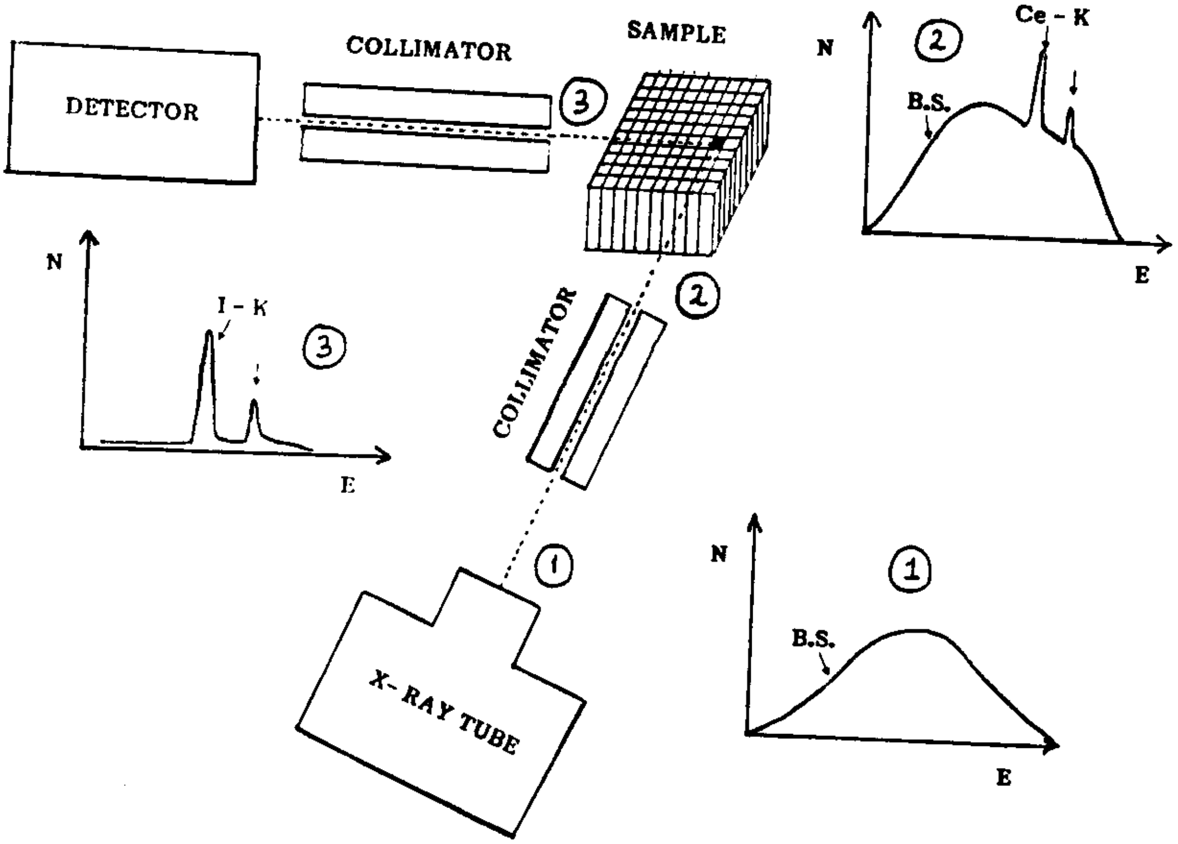

Figure 23 - Principles of the Fluorescent X-ray tomography.

6.1 Theoretical background

By irradiating a thick sample, for example a solution containing an element a with concentration C_a, with monoenergetic radiation of energy E_o and photon flux density N_o, and by detecting the X-rays of element a emitted at 90° with respect to the direction of the incident radiation, one can devide the section of the sample in many viewing elements (pixels) in which the attenuation of incident and output radiation is negligible. For pixels of about 1-2 mm^2 and elements with atomic number larger than about 40, each pixel can be considered as an infinitely thin sample, and X-rays emitted at 90° are given by: (ref. 7):

$$N_a = N_o K \omega_a \mu_{ph.a} m 0.71 C_a$$

where: N_o $(ph/cm^2 s)$ is the incident photon flux density

N_a $(ph/cm^2 s)$ is the fluorescent photon flux density of X-rays of element a

$K = \Omega_1 \; \Omega_2$ is the total geometrical factor, given by the product of source-sample solid angle Ω_2

ω_a is the fluorescent yield of element a in the shell of interest

$\mu_{ph.a}$ is the photoelectric absorption coefficient of element a at energy E_o

$m(g/cm^2)$ is the mass per unitary surface of the sample

Then is a linear relationship between the concentration C_a and the number of X-rays of element a, N_a.
Scattered counts N_{sc} are given by the Equation:

$$N_{sc} = N_o \; K \; \mu_{sc} \; m$$

given by:

$$\frac{N_a}{N_{sc}} = \frac{\omega_a \mu_{ph.a}\ 0.71\ Ca}{\mu_{sc}}$$

For a given element, for example a trace element in solution the ratio N_a/N_{sc} can be improved only by increasing the attenuation coefficient for photoelectric effect $\mu_{ph.a}$ because the attenuation coefficient of the matrix for scattering effects is practically constant.

6.2. Experimental arrangement

The experimental arrangement employed for the analysis of Iodine is shown in Figure 23. The bremsstrahlung radiation from the tube passes through a long collimator internally covered by cesium, in order to partially convert the primary radiation in Cs-X-rays, which energy lies just above the Iodine K-edge. With this geometrical arrangement, $K = \Omega_1 \Omega_2 = 1.3 \times 10^{-8}$; a very strong source is therefore needed.

The irradiated volume varies with the distance of the sample from the source and from the detector. It is therefore necessary to keep constant the position of the volume by moving the sample in the x-y axis. Calling m the pixel number in the x-axis and n in the y-axis, each pixel can be idenfied by a mn index. X-ray counts of element a have to be corrected for attenuation effects, both of incident radiation and of output radiation from the irradiated pixel. Counts in the detector related to the pixel mn are then given by:

$$N_{mn} = N_a \exp - \left\{ \sum_{h=1}^{m-1} \mu_{hn}(E_o)\ x \right\} \exp - \left\{ \sum_{h'=1}^{n-1} \mu_{mh'}(E_a)\ x \right\}$$

in which N_a is given by Equation .

A test object has been analyzed , constituted by a plexiglas matrix 20x20 mm^2 section, with 64 cylindrical holes of diameter $\emptyset = 2$ mm. The holes are empty, except those at the diagonal of the object, which are filled with a solution containing 0.5% Iodine. (Figure 24).

A second plexiglas test object has been employed, with the same external dimensions and with 4 cells machined in it;2 mm wide and 9 mm long, placed like an X figure along the diagonal of the object. In the center, a 4x4 mm^2 plexiglas area remained empty. In a second series of experiments, this sample has been analyzed, with the cells filled with a 0.5% Iodine solution. In this case, the attenuation effects on incident and output radiation has been considered, which depends on the position of the analyzed pixel. The results of the image reconstruction are shown in Figures25, before (25a) and after (25b) corrections for attenuation effects.

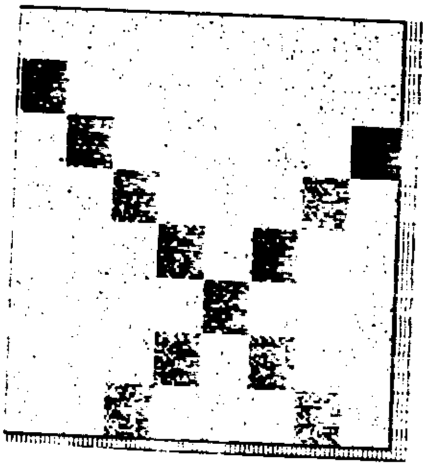

Figure 24 - Fluorescence X-Ray Tomography of a test object on plexiglas with holes, at the diagonal,filled with a solution containing 0.5% Iodine. The presence of Iodine in the image is evident.

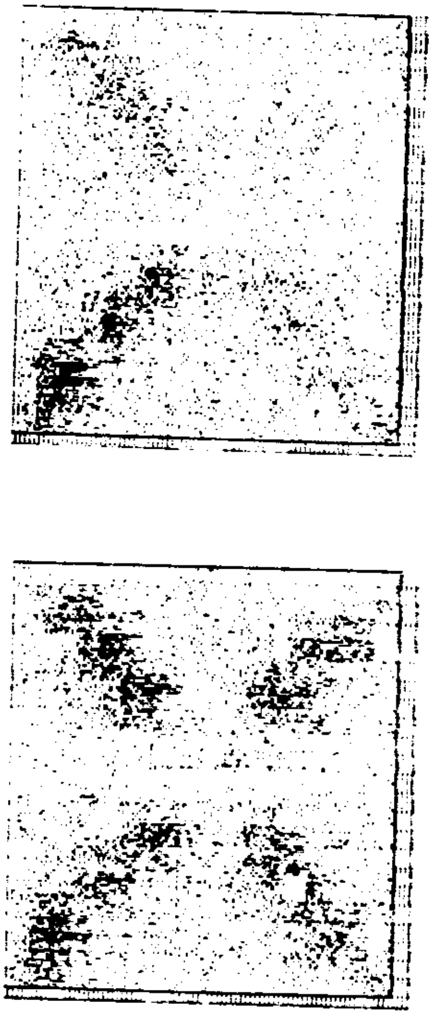

Figure 25 - Fluorescence X-Ray Tomography of a plexiglas test object with 4 cells 2 mm wide and 9 mm long, placed like an X Figure along the diagonals of the object, filled with a 0.5% solution. Figure 3A shows the direct results of the tomography and Figure 3B the same image after correction for the input and output radiation attenuation.

ACKNOWLEDGEMENTS

The author wish to thank Prof. Sergio Mascarenhas for useful discussion and for suggesting and co-operating to the Section 6.

Many thanks also to Dr. Lauro J. Pedraza for his co-operation to Section 2, and in particular for calculating the parameters S and F of coherent and incoherent scattering.

The author is also grateful to Dr. S.Q.G. Mahtaboally for useful discussion.

Many thanks also to the ICTP Programme for Training and Research in Italian Laboratories, Trieste and to Prof. Giuseppe Furlan Director of the Programme.

REFERENCES

1. J.H. Hubbell, Wm. J. Veigele, E.A. Briggs et al. J. Phys. Chem. Ref. Data 4 (1973) 471.
2. W.B. Gilboy, Nucl. Instrum. Methods in Phys. Res. 221 (1984) 193.
3. J.H. Radon, Bericht Sachs. Akadem. Wiss. 69 (1917) 262.
4. R. Cesareo, L. Pedraza, Nucl. Instrum. Methods in Phys. Res. A 239 (1985) 367.
5. R. Cesareo, Nucl. Instrum. Methods in Phys. Res. A 270 (1988) 572.
6. R. Cesareo, submitted to Nucl. Instrum. Methods.
7. R. Cesareo, "Photon induced X-Ray Emission" in Nuclear Analytical Techniques in Medicine (Ed. R. Cesareo), Elsevier (1988) 19.